

# Effect of Morphology on the Electrical Resistivity of Silver Nanostructure Films

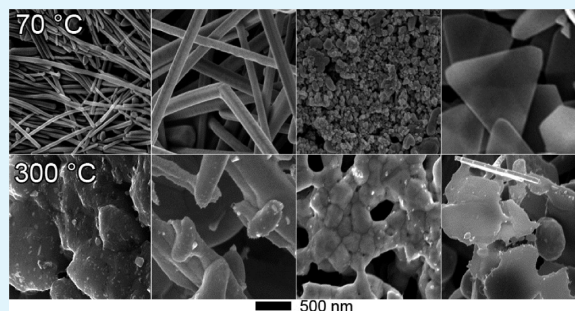
Ian E. Stewart, Myung Jun Kim, and Benjamin J. Wiley\*<sup>ID</sup>

Department of Chemistry, Duke University, 124 Science Drive, Box 90354, Durham, North Carolina 27708, United States

## **S** Supporting Information

**ABSTRACT:** The relatively high temperatures (>200 °C) required to sinter silver nanoparticle inks have limited the development of printed electronic devices on low-cost, heat-sensitive paper and plastic substrates. This article explores the change in morphology and resistivity that occurs upon heating thick films of silver nanowires (of two different lengths; Ag NWs), nanoparticles (Ag NPs), and microflakes (Ag MFs) at temperatures between 70 and 400 °C. After heating at 70 °C, films of long Ag NWs exhibited a resistivity of  $1.8 \times 10^{-5} \Omega \text{ cm}$ , 4000 times more conductive than films made from Ag NPs. This result indicates the resistivity of thick films of silver nanostructures is dominated by the contact resistance between particles before sintering. After sintering at 300 °C, the resistivity of short Ag NWs, long Ag NWs, and Ag NPs converge to a value of  $(2-3) \times 10^{-5} \Omega \text{ cm}$ , while films of Ag MFs remain  $\sim 10\times$  less conductive ( $4.06 \times 10^{-4} \Omega \text{ cm}$ ). Thus, films of long Ag NW films heated at 70 °C are more conductive than Ag NP films sintered at 300 °C. Adding 10 wt % nanowires to a film of nanoparticles results in a 400-fold improvement in resistivity.

**KEYWORDS:** silver nanowires, silver nanoparticles, silver microflakes, sintering, electrical resistivity



## 1. INTRODUCTION

Printed electronics manufactured through inkjet, aerosol, and screen printing technologies offer a low-cost alternative for electronic device manufacturing compared to traditional lithography, etching, vacuum, or electroless plating techniques.<sup>1</sup> With the market for printed electronics expected to reach \$300 billion over the next 20 years, research into better ways to print electronic devices for applications such as energy storage,<sup>2</sup> photovoltaics,<sup>3,4</sup> flexible electronics,<sup>5</sup> transistors,<sup>6</sup> and RFID tags<sup>7</sup> can provide information of considerable economic value. Polymers,<sup>8</sup> graphene,<sup>9</sup> and carbon nanotubes<sup>10</sup> have been demonstrated in conductive inks, but silver-based conductive inks continue to be one of the most widely used materials in printed electronics due to their oxidation resistance, water dispersibility, and low resistivity.<sup>1,11</sup>

The questions that we have sought to address in this work are, (1) what silver nanostructures result in the most conductive inks when deposited to form a thick film, and (2) how does the morphology and resistivity of these films depend on sintering temperature? Although silver nanowires (Ag NWs),<sup>12-15</sup> silver nanoparticles (Ag NPs),<sup>16-24</sup> and silver microflakes (Ag MFs)<sup>25-27</sup> have all been deposited from a variety of solutions to create printed lines with high conductivities, the solutions used to deposit these nanostructures and the temperatures used to sinter them vary from study to study (see Table 1). By using only water to deposit these various nanostructures, and by sintering them across a range of temperatures, we sought to obtain a more complete and

conclusive understanding of the relationship between morphology, temperature, and resistivity.

The most dramatic outcome from this study is the demonstration that films of Ag NWs are up to 4000 times more conductive than films of Ag NPs after drying at 70 °C. In fact, films of long Ag NWs dried at 70 °C are more conductive than films of Ag NPs sintered at 300 °C. As commercially available Ag NP inks have required high temperatures to make conductive lines, circuits made with such inks have to be printed on relatively costly polymer substrates that can withstand such temperatures, such as polyimide. This work demonstrates that the use of a Ag NW ink in place of a Ag NP ink will enable the printing of highly conductive traces or contacts on virtually any substrate.

## 2. RESULTS AND DISCUSSION

All four of the morphologies studied here were synthesized with previously reported literature methods. After synthesis, the nanowires, nanoparticles, and microflakes (Supporting Information Figure S1 shows XRD spectra of each morphology) were stored in distilled water and eventually deposited from these aqueous solutions into wells of known dimensions on a glass slide. Since the concentration of silver was known for each shape, the same amount of silver by mass was deposited into each well. The various shapes were then heated at 70 °C for 10

**Received:** September 27, 2016

**Accepted:** December 16, 2016

**Published:** December 16, 2016

**Table 1. Summary of Literature Values for the Resistivity of Ag NW, Ag NP, and Ag MF Films (IPA = Isopropanol, EG = Ethylene Glycol, HEC = Hydroxyethyl Cellulose, NF = Nanoflake, 2BE = 2-Butylethanol)<sup>a</sup>**

shape	dimens (shortest, longest)	drying temp (°C)	resistivity (Ω cm)	ink soln	ref
NW	60 nm, 15 μm	50	$2.6 \times 10^{-5}$	water	13
NW	55 nm, 2.2 μm	110	$1 \times 10^{-3}$	IPA + stabilizers	15
NW	100 nm, 5–10 μm	250	$2.1 \times 10^{-5}$	EG	12
<b>NW</b>	<b>48 nm, 6.2 μm</b>	<b>70</b>	<b><math>5.7 \times 10^{-5}</math></b>	<b>water</b>	<b>this work</b>
		<b>400</b>	<b><math>9.8 \times 10^{-6}</math></b>		
	<b>150 nm, 27 μm</b>	<b>70</b>	<b><math>1.8 \times 10^{-5}</math></b>	<b>water</b>	<b>this work</b>
NP	≤50 nm, –	320	$1.1 \times 10^{-4}$	water-based ink	22
NP	46 nm, –	250	$2.4 \times 10^{-5}$	water	20
NP	40 nm, –	180	$5 \times 10^{-6}$	organic-based ink	19
NP	12.2 nm, –	250	$4.5 \times 10^{-6}$	ethanol-based solvents	21
NP	400 nm, –	200	$4.34 \times 10^{-6}$	ethanol and HEC	28
NP	40 nm, –	180	$3.7 \times 10^{-6}$	water and EG	24
NP	12 nm, –	250	$3.8 \times 10^{-6}$	tetradecane	23
<b>NP</b>	<b>27 nm, –</b>	<b>400</b>	<b><math>2.4 \times 10^{-5}</math></b>	<b>water</b>	<b>this work</b>
NF	–, 35 nm	200	$9.4 \times 10^{-6}$	EG and 2BE	25
NF	30 nm, 517 nm	200	$7.4 \times 10^{-6}$	ethanol	27
<b>MF</b>	<b>51 nm, 1.6 μm</b>	<b>250</b>	<b><math>9.3 \times 10^{-5}</math></b>	<b>water</b>	<b>this work</b>

<sup>a</sup>Entries in bold are from this work.

min to remove any moisture and then separately placed in a tube furnace at 200, 250, 300, and 400 °C for 30 min. The sheet resistance was measured after the samples cooled to room temperature.

The mass of deposited silver and the measured sheet resistance of the films were used to calculate resistivity with the following equation:

$$\rho = R_s \frac{m}{\rho_{\text{Ag}} \pi r^2}$$

where  $\rho$  is the resistivity of the film,  $R_s$  is sheet resistance,  $m$  is the mass of silver species,  $\rho_{\text{Ag}}$  is the density of silver, and  $r$  is the radius of the well. We note that some other publications determine the resistivity of the film with the following equation:

$$\rho = R_s t$$

where  $t$  is the film thickness measured with a profilometer or SEM. We chose not to do it this way for three reasons. First, given the natural roughness of the silver films, the determination of mass in a film can be made to a greater precision than the determination of the film thickness. Second, we are principally interested in the film resistance as a function of silver mass since we believe more people are interested in minimizing the mass of silver used to achieve a given line resistance and generally do not seek to minimize the thickness of a printed line necessary to achieve a given resistance. Third, different nanostructures will lead to very different film thicknesses given the same mass of silver. For example, the thickness of the silver nanoparticle films are less than half that of the silver nanowire films of the same mass, meaning that the silver nanowire films have roughly twice the porosity (Table S1 shows the experimental thicknesses and surface roughnesses of the films determined via profilometer). Obviously, the Ag NW films do not have twice the amount of silver, so it does not make sense to use the thicknesses of these two films to compare their resistivities. Thus, we used the mass of silver in the films discussed here to calculate an effective thickness, and used this thickness to determine the resistivity of the films.

Figure 1 shows SEM images of short Ag NWs (length =  $6.2 \pm 2.4 \mu\text{m}$ ; diameter =  $48 \pm 10 \text{ nm}$ ) after heating at various

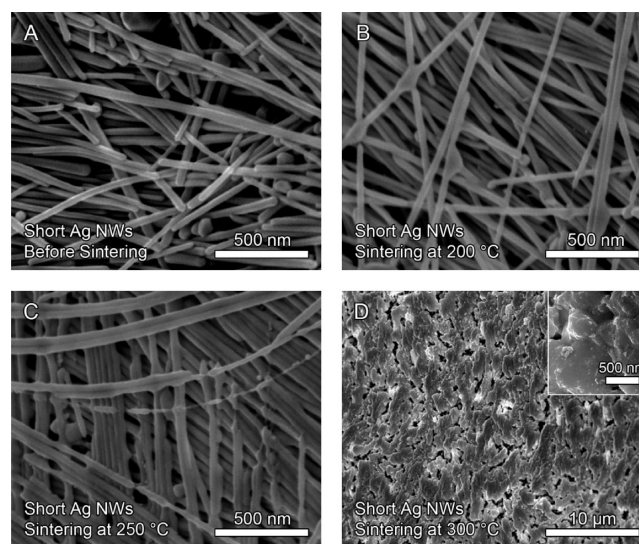


**Figure 1.** SEM images of short Ag NWs (length =  $6.2 \pm 2.4 \mu\text{m}$ ; diameter =  $48 \pm 10 \text{ nm}$ ) after (A) removal of water at 70 °C for 10 min and sintering at (B) 200, (C) 250, and (D) 300 °C for 30 min.

temperatures. After drying at 70 °C there was no visible sintering between the nanowires (Figure 1A). After heating at 200 °C (Figure 2B), the nanowires began to sinter at nanowire–nanowire contacts. When the sintering temperature was increased to 250 °C, nanowires began to deform into particles (Figure 1C).<sup>29</sup> At 300 °C the short nanowires melted into a porous film of silver (Figure 1D).

Junction resistance between nanowires in a network has been shown to dominate the overall resistance of a thin, nanowire-based transparent conducting film.<sup>30–34</sup> Limiting the number of junctions in a film of a given mass requires longer nanowires.<sup>35</sup> To examine this phenomenon in dense films of nanowires, we made films from Ag NWs with an average length =  $27 \pm 12 \mu\text{m}$  (diameter =  $150 \pm 30 \text{ nm}$ ) for comparison with the films made from the shorter Ag NWs with an average length of  $6.2 \pm 2.4 \mu\text{m}$  (see Figure S2 for dark field optical microscopy images of the short and long Ag NWs). Figure 2 shows the morphology

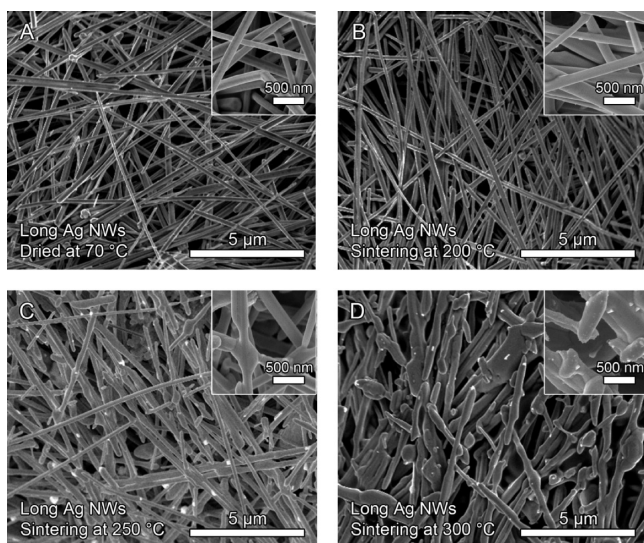
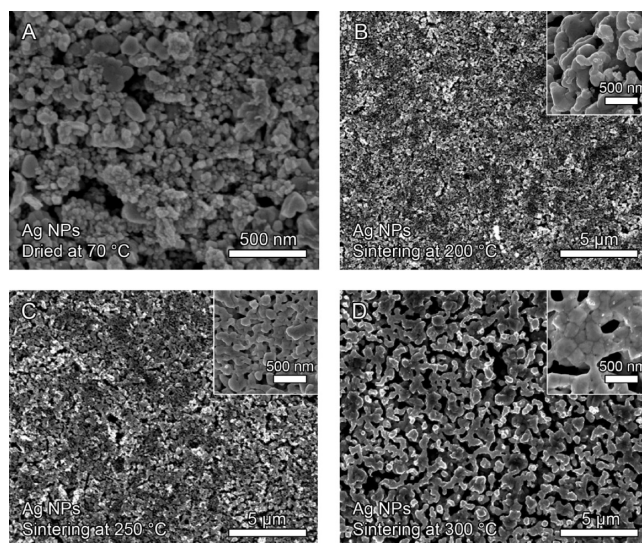


**Figure 2.** SEM images of long Ag NWs (length =  $27 \pm 12 \mu\text{m}$ ; diameter =  $150 \pm 30 \text{ nm}$ ) after (A) water removal at  $70 \text{ }^\circ\text{C}$  for 10 min and sintering at (B) 200, (C) 250, and (D)  $300 \text{ }^\circ\text{C}$  for 30 min.

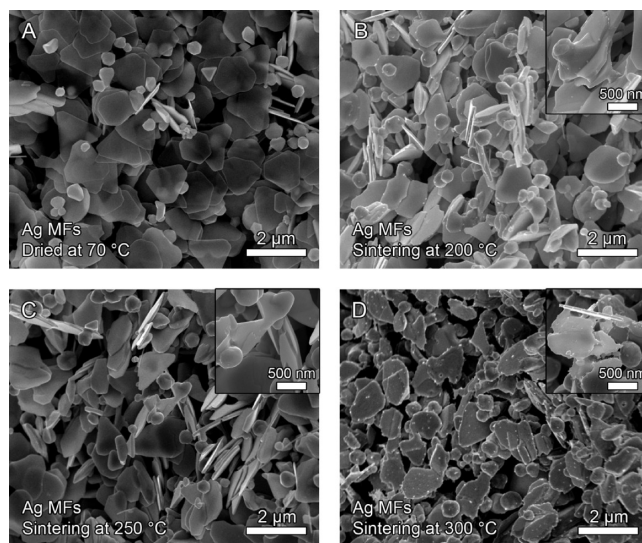
of the long Ag NWs before (Figure 2A) and after sintering. At  $200 \text{ }^\circ\text{C}$  (Figure 2B) the long Ag NWs sintered at nanowire–nanowire contacts, but to a lesser extent than for the short Ag NWs. At  $250 \text{ }^\circ\text{C}$  (Figure 2C) the long Ag NWs maintain their cylindrical shape with some slight curvature along the length of some nanowires. The difference between the long and short nanowires was even more apparent at  $300 \text{ }^\circ\text{C}$  (Figure 2D) as the long Ag NWs clearly still resembled nanowires. In contrast, the short Ag NWs melted under these conditions. This difference was due to the larger diameter of the long Ag NWs; the temperature required for spheroidization of nanowires due to Rayleigh instability increases with nanowire diameter.<sup>29,36</sup> This instability is dependent on surface diffusion, and because there is a higher ratio of surface atoms on the smaller diameter Ag NWs compared to the larger diameter long Ag NWs, the former break apart into spheres at a lower temperature. For example, Langley et al.<sup>29</sup> showed that transparent films of Ag NWs with diameters of  $25 \text{ nm}$  lost conductivity (broke into spheres) at  $225 \text{ }^\circ\text{C}$ , but Ag NWs with diameters of  $117 \text{ nm}$  did not do so below  $275 \text{ }^\circ\text{C}$ . Similarly, the short Ag NWs in this study (diameter =  $48 \text{ nm}$ ) began to break apart around  $250 \text{ }^\circ\text{C}$ , but the long Ag NWs (diameter =  $150 \text{ nm}$ ) did not exhibit this instability until closer to  $300 \text{ }^\circ\text{C}$ .

Figure 3 shows the effects of sintering on dense films of Ag NPs (average particle size =  $27 \pm 8 \text{ nm}$ ). After drying at  $70 \text{ }^\circ\text{C}$  for 10 min (Figure 3A), no evidence of sintering between the Ag NPs was observed. At  $200 \text{ }^\circ\text{C}$  (Figure 3B) and  $250 \text{ }^\circ\text{C}$  (Figure 3C) the nanoparticles clearly started to melt together to form an interconnected network of particles. At  $300 \text{ }^\circ\text{C}$  the Ag NPs merged further, resulting in enlarged contacts between nanoparticles. The fact that the Ag NPs melt sooner than the Ag NWs is expected considering their greater radius of curvature, which results in a stronger driving force for particle growth and diffusion of silver to contacts.

Finally, Ag MFs (length =  $1.6 \pm 0.3 \mu\text{m}$ ; thickness =  $51 \pm 8 \text{ nm}$ ) underwent identical sintering treatments as the previous silver shapes. Figure 4A shows the random orientation of the flakes in the film after drying at  $70 \text{ }^\circ\text{C}$ . At  $200 \text{ }^\circ\text{C}$  (Figure 4B) and  $250 \text{ }^\circ\text{C}$  (Figure 4C) significant necking began to occur between nanoparticles and the smaller, sharper corners of the



**Figure 3.** SEM images of Ag NPs (diameter =  $27 \pm 8 \text{ nm}$ ) after (A) water removal at  $70 \text{ }^\circ\text{C}$  for 10 min and sintering at (B) 200, (C) 250, and (D)  $300 \text{ }^\circ\text{C}$  for 30 min.



**Figure 4.** SEM images of Ag MFs (length =  $1.6 \pm 0.3 \mu\text{m}$ ; thickness =  $51 \pm 8 \text{ nm}$ ) after (A) water removal at  $70 \text{ }^\circ\text{C}$  for 10 min and sintering at (B) 200, (C) 250, and (D)  $300 \text{ }^\circ\text{C}$  for 30 min.

Ag MFs. At  $300 \text{ }^\circ\text{C}$  (Figure 4D) the Ag MFs themselves began to melt and deform, but sintering between the stacked faces of the flakes was not observed. Instead, flakes melted along their edges, and this did not appear to increase the contact area between particles.

The morphological changes of the silver nanostructures associated with an increase in sintering temperature can be directly correlated to the change in resistivity of the films as a function of temperature (Figure 5). After deposition from water and drying at  $70 \text{ }^\circ\text{C}$  for 10 min, all of the morphologies formed conductive films. However, films of the Ag NWs were orders of magnitude more conductive than nanoparticles or microflakes. The resistivity of the Ag NW films ( $1.76 \times 10^{-5} \Omega \text{ cm}$ ) was only 10 times that of bulk silver ( $\rho = 1.6 \times 10^{-6} \Omega \text{ cm}$ ). This is the lowest resistivity for Ag NWs deposited from water and dried at low temperatures ( $<100 \text{ }^\circ\text{C}$ ). The short Ag NWs were also quite conductive prior to sintering ( $\rho = 5.71 \times 10^{-5} \Omega \text{ cm}$ )

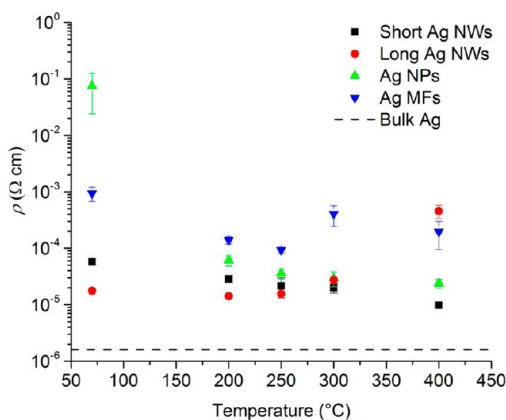


**Figure 5.** Resistivity versus sintering temperature for various silver nanomorphologies. See Table S2 for tabulated values.

but slightly less so than the long Ag NWs. It is likely this difference was due to the fact that electrons must traverse a larger number of nanowire–nanowire contacts in films of short nanowires. The junction resistance has previously been shown to dominate the resistivity of nanowire-based transparent conductive films.<sup>30–34</sup> Here we are seeing that the junction resistance dominates the resistivity of thick films of nanowires as well, at least prior to sintering.

After sintering at 200 °C the resistivities of each morphology decreased by various amounts due to sintering of the contacts between the nanostructures. Once again the long Ag NWs exhibited the lowest resistivity ( $\rho = 1.42 \times 10^{-5} \Omega \text{ cm}$ ), but now the short Ag NWs were only about half as conductive ( $\rho = 2.88 \times 10^{-5} \Omega \text{ cm}$ ). The relative degrees to which the Ag NWs became more conductive after sintering are likely due to a greater degree of sintering between the short nanowires. The resistivity decrease for the Ag NPs ( $\rho = 6.07 \times 10^{-5} \Omega \text{ cm}$ ) and Ag MFs ( $\rho = 1.4 \times 10^{-5} \Omega \text{ cm}$ ) is much more dramatic compared to the nanowires. Examining Figures 3B and 4B, one can attribute this drop to the melting of particles into larger shapes and the necking between flakes, both of which decrease the resistivity of contact points throughout the films.

The relative resistivities of the films ( $\rho_{\text{long Ag NWs}} < \rho_{\text{short Ag NWs}} < \rho_{\text{Ag NPs}} < \rho_{\text{Ag MFs}}$ ) did not change when the sintering temperature was increased to 250 °C. The Ag NPs and Ag MFs both become slightly more conductive ( $3.58 \times 10^{-5}$  and  $9.28 \times 10^{-5} \Omega \text{ cm}$ , respectively) due to diffusion of silver to interparticle contacts. The Ag MFs have a slightly higher resistivity since contacts between flakes are only being made at the edges of flakes, whereas the Ag NPs sintered into a porous network. The resistivity of short Ag NW films decreases slightly from 200 to 250 °C ( $2.88 \times 10^{-5}$  to  $2.15 \times 10^{-5} \Omega \text{ cm}$ ) while the long Ag NWs remain at roughly the same level (the increase in resistivity from  $1.42 \times 10^{-5}$  to  $1.56 \times 10^{-5} \Omega \text{ cm}$  is within error). In Figures 1C and 2C both sets of nanowires look as if they are beginning to transform into nanoparticles due to Rayleigh instability. The fact that this instability did not increase the resistivity of the films suggests that further sintering at contacts offsets any reduction in conductivity due to nanowire deformation.

At 300 °C, the short Ag NWs, long Ag NWs, and Ag NPs all exhibit resistivity values within error of one another:  $\rho_{\text{short Ag NWs}} = 2.0 \times 10^{-5} \Omega \text{ cm}$ ,  $\rho_{\text{long Ag NWs}} = 2.74 \times 10^{-5} \Omega \text{ cm}$ , and  $\rho_{\text{Ag NPs}} = 2.93 \times 10^{-5} \Omega \text{ cm}$ . At this point, the surface diffusion of silver to the contacts between Ag NPs has enlarged the contact area

between nanoparticles to be comparable to the diameter of the nanowires, resulting in similar resistivities for films of these nanostructures. The resistivities of the short Ag NWs and Ag NPs decrease slightly from their values at 250 °C due to almost complete melting of the silver to form a porous conductive sheet. The small increase in resistivity of the long Ag NWs was most likely due to continued melting and destruction of the nanowires, but their diameters are too large for the nanowires to melt completely to form a continuous porous film at 300 °C. Similarly, the Ag MFs begin to melt and lose their shape at this temperature, resulting in an apparent decrease in the number and extent of contacts between particles, and a decrease in conductivity ( $\rho = 4.06 \times 10^{-4} \Omega \text{ cm}$ ).

Although 400 °C is a higher temperature than would be used in the majority of practical applications, it is instructive to observe what further changes in morphology and resistivity occurred. The short Ag NWs (Figure 6A) melted to form a

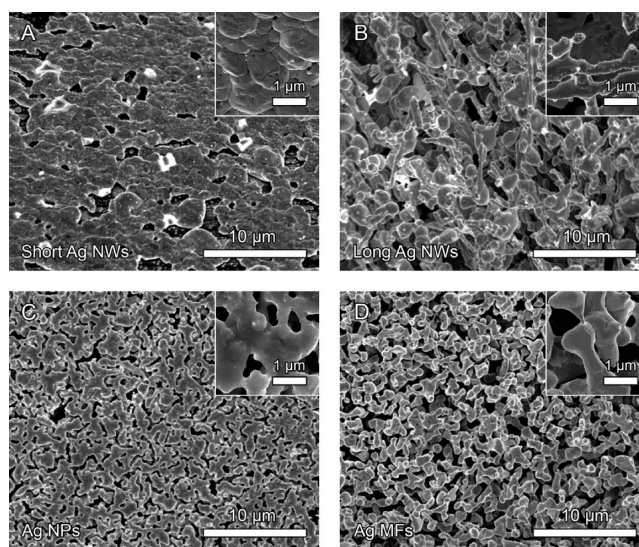


**Figure 6.** SEM images of (A) short Ag NWs, (B) long Ag NWs, (C) Ag NPs, and (D) Ag MFs sintered at 400 °C.

continuous film of silver resulting in a resistivity of  $9.77 \times 10^{-6} \Omega \text{ cm}$  which is  $\sim 6$  times the resistivity of bulk silver. The long Ag NWs (Figure 6B) continue to degrade without melting completely at this temperature, causing their resistivity to climb to  $4.56 \times 10^{-4} \Omega \text{ cm}$ . The resistivity of the Ag NPs ( $\rho = 4.56 \times 10^{-4} \Omega \text{ cm}$ ) falls slightly from its value at 300 °C but remains within error as the nanoparticles melt and form an interconnected, porous film (Figure 6C). The film of Ag MFs becomes more conductive at 400 °C as the temperature was high enough to induce complete melting of the microflakes to form an interconnected network somewhat similar to, but more porous than, the film of Ag NPs.

Finally, we mixed Ag NPs with the long Ag NWs and sintered at 200 °C to see to what degree filling pore space and/or improving local sintering between nanowires with nanoparticles could improve the resistivity of this film. Panels A and B of Figure 7 show films of 10:90 (mass ratio) Ag NPs:long Ag NWs before and after sintering at 200 °C. At this concentration the Ag NPs primarily cluster along the nanowires. While the resistivity of the 10:90 Ag NP:Ag NW film dried at 70 °C is slightly higher than the film of just long Ag NWs at the same temperature ( $7.4 \times 10^{-5} \Omega \text{ cm}$  versus  $1.76 \times 10^{-5} \Omega \text{ cm}$ , respectively), it is orders of magnitude lower than a film of

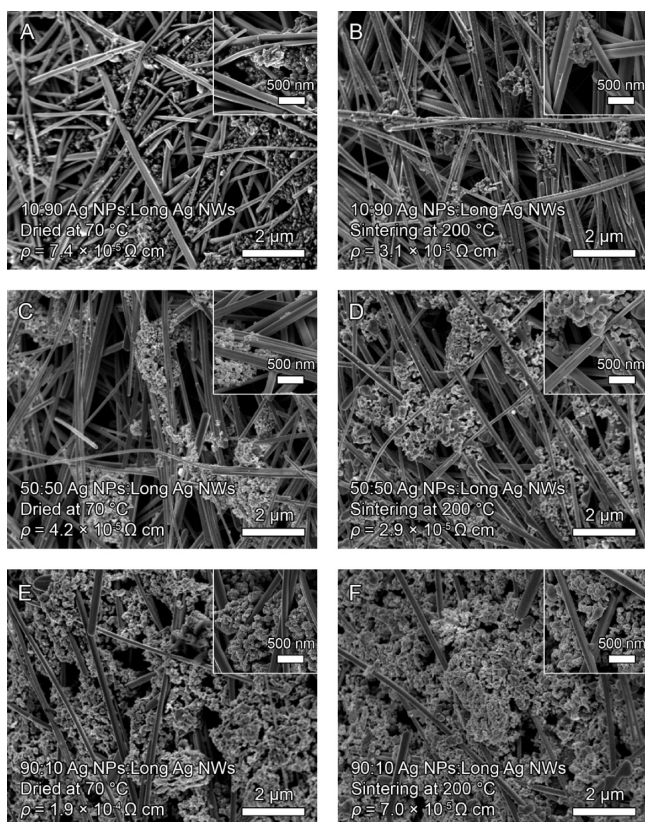


**Figure 7.** SEM images of 10:90 Ag NP:long Ag NW mixtures (A) dried at 70 °C and (B) sintered at 200 °C; 50:50 Ag NP:long Ag NW mixtures (C) dried at 70 °C and (D) sintered at 200 °C; and 90:10 Ag NP:long Ag NW mixtures (E) dried at 70 °C and (F) sintered at 200 °C.

pure, dried Ag NPs ( $\rho = 7.51 \times 10^{-2} \Omega \text{ cm}$ ) since there are less nanoparticle–nanoparticle contacts to lower the conductivity. Although sintering the films at 200 °C improves the resistivity slightly ( $\rho = 3.1 \times 10^{-5} \Omega \text{ cm}$ ), the melted Ag NPs do not assist in sintering at nanowire–nanowire contacts enough to lower the film resistivity below that of pure long Ag NWs. A similar result is seen when the Ag NP fraction is increased to 50% in that the resistivity of the 50:50 films before ( $4.2 \times 10^{-5} \Omega \text{ cm}$ ) sintering (Figure 7C) is not below that of the pure long Ag NW films, but a large decrease in resistivity is seen when compared to the dried Ag NPs. After sintering at 200 °C ( $\rho = 2.9 \times 10^{-5} \Omega \text{ cm}$ , Figure 7D) the resistivity is double the value for the pure long Ag NW films, but again lower than the pure Ag NP films. In this case the Ag NPs are still mostly clustering along the nanowires but fill the void areas between the nanowires to a greater degree than the 10:90 Ag NP:long Ag NW films. Finally, films of 90:10 Ag NPs:long Ag NWs were dried at 70 °C (Figure 7E) and sintered at 200 °C (Figure 7F). After drying, these films had a resistivity of  $1.9 \times 10^{-4} \Omega \text{ cm}$ , the highest of any of the mixtures due to the significant Ag NP portion. However, it is interesting to note that the addition of only 10% weight by mass of Ag NWs improved the conductivity of Ag NP films by almost 3 orders of magnitude, again highlighting the significance of the incorporation of a small fraction of high aspect ratio conductive material into a percolative network. This result is similar to previously observed effects of adding long nanowires to short nanowires in transparent conductive films.<sup>33,37</sup> When sintered at 200 °C,

the 90:10 mixture has a resistivity of  $7 \times 10^{-5} \Omega \text{ cm}$ , almost identical to the pure Ag NP films at this temperature ( $6.07 \times 10^{-5} \Omega \text{ cm}$ ).

We note that none of the resistivities of the mixed films are lower than the resistivity of a film of pure, long Ag NWs dried from solution at 70 °C, which we presume did not undergo any sintering. Thus, we again conclude that a pure film of long nanowires is the best morphology for efficient electron transport at low sintering temperatures due to the low number of internanoparticle contacts. No degree of pore-filling or additional sintering provided by nanoparticles offsets the poor electron transport through the partially sintered nanoparticle networks.

### 3. CONCLUSION

In summary, we have shown that long Ag NWs have the lowest resistivity compared to Ag NPs and Ag MFs when deposited from water and dried at 70 °C. Films of Ag NWs dried at 70 °C are up to 4000 times more conductive than films of Ag NPs after drying at 70 °C and are more conductive than films of Ag NPs sintered at 300 °C. When sintered at 400 °C, short Ag NWs can reach resistivity values 6 times that of bulk silver. Without using film formers or organic additives we were able to compare and contrast the effect of morphology on the resistivity of thick silver nanostructure films. As with transparent conductors, the junction resistance of the conductive material in a dense film is crucial for determining the overall resistance of the deposited network. These results should benefit those searching for enhanced conductivity from printed electronics by optimizing the conductive filler morphology within the printable ink.

### 4. EXPERIMENTAL METHODS

#### 4.1. Synthesis of Various Silver Nanomorphologies.

**4.1.1. Short Nanowire Synthesis.** Short Ag NWs (length =  $6.2 \pm 2.4 \mu\text{m}$ ; diameter =  $48 \pm 10 \text{ nm}$ ) were synthesized according to the polyol method.<sup>38</sup> First, 158.4 mL of ethylene glycol (EG, J.T. Baker) was added to a 500 mL round-bottom flask which was subsequently stoppered and heated to 130 °C in an oil bath for 1 h. The following solutions were then prepared: (1) 0.257 g of NaCl (Fischer Scientific) in 20 mL of EG, (2) 0.081 g of  $\text{Fe}(\text{NO}_3)_3$  (Aldrich) in 10 mL of EG, (3) 1.05 g of PVP (MW = 55,000; Aldrich) in 25 mL of EG, and (4) 1.05 g of  $\text{AgNO}_3$  (Fischer Scientific) in 25 mL of EG. Next, 0.2 mL of solution 1, 0.1 mL of solution 2, 20.76 mL of solution 3, and 20.76 mL of solution 4 were added to the preheated 500 mL flask in that order with about 30 s between each addition. The flask was then stoppered, and the reaction was allowed to stir at 250 rpm and 130 °C for 6 h. Finally, the short Ag NWs were purified by washing twice with acetone (VWR) and once with water and were stored in water.

**4.1.2. Long Nanowire Synthesis.** Long Ag NWs ( $L = 27 \pm 12 \mu\text{m}$ ;  $D = 150 \pm 30 \text{ nm}$ ) were synthesized via the same polyol method described above except the solution of EG was preheated to 125 °C for 1 h and left at this temperature for 5 min after the four solutions had been added. After these 5 min were over, the oil bath temperature was raised to 130 °C and the contents were left stirring at 150 rpm for 6 h. The washing and storage procedure was also the same as for the short Ag NWs.

**4.1.3. Silver Nanoparticle Synthesis.** Ag NPs (average particle size =  $27 \pm 8 \text{ nm}$ ) were synthesized following the procedure by Magdassi et al.<sup>18</sup> In a 50 mL round-bottom flask, 4.5 g of  $\text{AgC}_2\text{H}_3\text{O}_2$  (Aldrich), 2.9 g of 20% poly(acrylic acid) (diluted from 40% poly(acrylic acid), MW = 8000; Aldrich), and 28 mL of distilled water were combined and heated to 95 °C for 15 min while stirring. Next, 3.4 g of 30 wt % ascorbic acid (Aldrich) were added to the flask and the mixture was heated and stirred for 30 min. The Ag NPs were washed with and stored in distilled water.

**4.1.4. Silver Microflake Synthesis.** A scaled up version of the seeded synthesis by Audoit et al.<sup>26</sup> was used to synthesize Ag MFs (length =  $1.6 \pm 0.3 \mu\text{m}$ ; thickness =  $51 \pm 8 \text{ nm}$ ). First, silver seeds were synthesized by mixing 24 mL of sodium citrate dihydrate (0.2 mM, Aldrich), 0.06 mL of  $\text{AgNO}_3$  (0.025 M, Aldrich), 0.06 mL of iced  $\text{H}_2\text{O}_2$  (2.418 M, Acros Organics), and 0.08 mL of distilled water followed by the dropwise addition of fresh, cold 0.8 mL of  $\text{NaBH}_4$  (0.05 M, Alfa Aesar) under vigorous stirring. The mixture was allowed to stir for an additional 3 min, and the resulting yellow solution was collected without purification. These silver seeds (2 mL) were added to 8 mL of distilled water, 0.5 mL of sodium citrate dihydrate, and 1 mL of ascorbic acid (0.1 M, Aldrich) while stirring. To synthesize silver nanoplates, 0.3 mL of  $\text{AgNO}_3$  (0.01 M) was added to this mixture via syringe pump at a rate of  $3.0 \text{ mL h}^{-1}$ . The resulting blue solution of silver nanoplates was used in the next step without purification. To a 500 mL flask, 10 mL of silver nanoplates, 90 mL of distilled water, and 100 mL of ascorbic acid (0.008 M) and sodium citrate dihydrate (0.00267 M) were combined under moderate stirring. Then 100 mL of  $\text{AgNO}_3$  (0.004 M) were injected into the flask via syringe pump at a rate of  $55 \text{ mL h}^{-1}$ . Once the addition of  $\text{AgNO}_3$  was complete, 100 mL of the gray colored product were added to a clean round-bottom flask (without purification) with 100 mL of ascorbic acid (0.008 M) and sodium citrate dihydrate (0.00267 M) while stirring. Again, 100 mL of  $\text{AgNO}_3$  (0.004 M) was injected into this flask via syringe pump at a rate of  $67 \text{ mL h}^{-1}$  while stirring. This process was completed once more with a  $\text{AgNO}_3$  addition rate of  $100 \text{ mL h}^{-1}$ . Finally, 30 mL of  $\text{NaOH}$  (0.5 M Acros Organics) was added to the microflakes, and they were collected by washing three times with distilled water.

**4.2. Film Fabrication and Sintering Experiments.** Wells were constructed from 0.12 mm thick double sided tape by using a 7 mm diameter hole punch and adhering the tape to glass slides. For both nanowire shapes and the microflakes, the glass slides were pretreated by sonicating in acetone then IPA; this was not necessary for the nanoparticles. The short nanowires, particles, and microflakes were concentrated to  $20 \text{ mg mL}^{-1}$  and deposited from water into separate wells (0.05 mL of solution). These wells were then placed in an oven at  $70 \text{ }^\circ\text{C}$  to remove the water and finally placed in a tube furnace at the desired temperature ( $200\text{--}400 \text{ }^\circ\text{C}$ ). Since the long nanowires would aggregate at higher concentrations,  $0.05 \text{ mL}$  of  $2 \text{ mg mL}^{-1}$  were deposited into the wells and then dried at  $70 \text{ }^\circ\text{C}$ . This was repeated for a total of 10 times in order for the mass of silver deposited to match the other morphologies ( $1 \text{ mg}$ ).

**4.3. Instrumentation and Characterization.** Dark field optical microscopy (DFOM) images were taken with an Olympus BX51 microscope. SEM (FEI XL30 SEM-FEG) images and XRD (Panalytical X'Pert PRO MRD HR XRD) spectra were taken at the Shared Materials Instrumentation Facility at Duke University. Metal concentration measurements were completed using a PerkinElmer 3100 atomic absorption spectrophotometer (AAS). For all films sheet resistance values were measured using a four-point probe (Signatone SP4-50045TBS) and thicknesses were calculated from the mass of silver deposited.

## ■ ASSOCIATED CONTENT

### 📄 Supporting Information

The Supporting Information is available free of charge on the ACS Publications website at DOI: [10.1021/acsami.6b12289](https://doi.org/10.1021/acsami.6b12289).

XRD spectra of synthesized silver morphologies, DFOM images of long and short Ag NWs, a table of the thickness and roughness of silver nanostructure films, and tabulated resistivity values for the data points in Figure 5 (PDF)

## ■ AUTHOR INFORMATION

### Corresponding Author

\*E-mail: [benjamin.wiley@duke.edu](mailto:benjamin.wiley@duke.edu).

## ORCID

Benjamin J. Wiley: [0000-0003-0055-9018](https://orcid.org/0000-0003-0055-9018)

## Notes

The authors declare no competing financial interest.

## ■ ACKNOWLEDGMENTS

I.E.S. was supported by a GAANN Fellowship through the Duke Chemistry Department. This work was supported by NSF Grant No. ECCS-1344745 and an NSF CAREER award (DMR-1253534).

## ■ REFERENCES

- (1) Kamyshny, A.; Magdassi, S. Conductive Nanomaterials for Printed Electronics. *Small* **2014**, *10*, 3515–3535.
- (2) Hu, L.; Choi, J. W.; Yang, Y.; Jeong, S.; La Mantia, F.; Cui, L.-F.; Cui, Y. Highly Conductive Paper for Energy-Storage Devices. *Proc. Natl. Acad. Sci. U. S. A.* **2009**, *106*, 21490–21494.
- (3) Hoth, C. N.; Choulis, S. A.; Schilinsky, P.; Brabec, C. J. High Photovoltaic Performance of Inkjet Printed Polymer:Fullerene Blends. *Adv. Mater.* **2007**, *19*, 3973–3978.
- (4) Krebs, F. C.; Tromholt, T.; Jorgensen, M. Upscaling of Polymer Solar Cell Fabrication Using Full Roll-to-Roll Processing. *Nanoscale* **2010**, *2*, 873–886.
- (5) Rogers, J. A.; Someya, T.; Huang, Y. Materials and Mechanics for Stretchable Electronics. *Science* **2010**, *327*, 1603–1607.
- (6) Sirringhaus, H.; Kawase, T.; Friend, R. H.; Shimoda, T.; Inbasekaran, M.; Wu, W.; Woo, E. P. High-Resolution Inkjet Printing of All-Polymer Transistor Circuits. *Science* **2000**, *290*, 2123–2126.
- (7) Subramanian, V.; Frechet, J. M. J.; Chang, P. C.; Huang, D. C.; Lee, J. B.; Molesa, S. E.; Murphy, A. R.; Redinger, D. R.; Volkman, S. K. Progress Toward Development of All-Printed RFID Tags: Materials, Processes, and Devices. *Proc. IEEE* **2005**, *93*, 1330–1338.
- (8) Garnier, F.; Hajlaoui, R.; Yassar, A.; Srivastava, P. All-Polymer Field-Effect Transistor Realized by Printing Techniques. *Science* **1994**, *265*, 1684–1686.
- (9) Torrisi, F.; Hasan, T.; Wu, W.; Sun, Z.; Lombardo, A.; Kulmala, T. S.; Hsieh, G.-W.; Jung, S.; Bonaccorso, F.; Paul, P. J.; Chu, D.; Ferrari, A. C. Inkjet-Printed Graphene Electronics. *ACS Nano* **2012**, *6*, 2992–3006.
- (10) Park, S.; Vosguerichian, M.; Bao, Z. A Review of Fabrication and Applications of Carbon Nanotube Film-Based Flexible Electronics. *Nanoscale* **2013**, *5*, 1727–1752.
- (11) Magdassi, S.; Bassa, A.; Vinetsky, Y.; Kamyshny, A. Silver Nanoparticles as Pigments for Water-Based Ink-Jet Inks. *Chem. Mater.* **2003**, *15*, 2208–2217.
- (12) Komoda, N.; Nogi, M.; Sukanuma, K.; Kohno, K.; Akiyama, Y.; Otsuka, K. Printed Silver Nanowire Antennas With Low Signal Loss at High-Frequency Radio. *Nanoscale* **2012**, *4*, 3148–3153.
- (13) Yang, C.; Gu, H.; Lin, W.; Yuen, M. M.; Wong, C. P.; Xiong, M.; Gao, B. Silver Nanowires: From Scalable Synthesis to Recyclable Foldable Electronics. *Adv. Mater.* **2011**, *23*, 3052–3056.
- (14) Song, L.; Myers, A. C.; Adams, J. J.; Zhu, Y. Stretchable and Reversibly Deformable Radio Frequency Antennas Based on Silver Nanowires. *ACS Appl. Mater. Interfaces* **2014**, *6*, 4248–4253.
- (15) Finn, D. J.; Lotya, M.; Coleman, J. N. Inkjet Printing of Silver Nanowire Networks. *ACS Appl. Mater. Interfaces* **2015**, *7*, 9254–9261.
- (16) Li, Y.; Wu, Y.; Ong, B. S. Facile Synthesis of Silver Nanoparticles Useful for Fabrication of High-Conductivity Elements for Printed Electronics. *J. Am. Chem. Soc.* **2005**, *127*, 3266–3267.
- (17) Perelaer, J.; de Gans, B. J.; Schubert, U. S. Ink-jet Printing and Microwave Sintering of Conductive Silver Tracks. *Adv. Mater.* **2006**, *18*, 2101–2104.
- (18) Magdassi, S.; Grouchko, M.; Berezin, O.; Kamyshny, A. Triggering the Sintering of Silver Nanoparticles at Room Temperature. *ACS Nano* **2010**, *4*, 1943–1948.

- (19) Greer, J. R.; Street, R. A. Thermal Cure Effects on Electrical Performance of Nanoparticle Silver Inks. *Acta Mater.* **2007**, *55*, 6345–6349.
- (20) Lee, H.-H.; Chou, K.-S.; Huang, K.-C. Inkjet Printing of Nanosized Silver Colloids. *Nanotechnology* **2005**, *16*, 2436–2441.
- (21) Jung, I.; Shin, K.; Kim, N. R.; Lee, H. M. Synthesis of Low-Temperature-Processable and Highly Conductive Ag Ink by a Simple Ligand Modification: The Role of Adsorption Energy. *J. Mater. Chem. C* **2013**, *1*, 1855–1862.
- (22) Kamyshny, A.; Ben-Moshe, M.; Aviezer, S.; Magdassi, S. Ink-Jet Printing of Metallic Nanoparticles and Microemulsions. *Macromol. Rapid Commun.* **2005**, *26*, 281–288.
- (23) Ryu, K.; Moon, Y.-J.; Park, K.; Hwang, J.-Y.; Moon, S.-J. Electrical Property and Surface Morphology of Silver Nanoparticles After Thermal Sintering. *J. Electron. Mater.* **2016**, *45*, 312–321.
- (24) Shen, W.; Zhang, X.; Huang, Q.; Xu, Q.; Song, W. Preparation of Solid Silver Nanoparticles for Inkjet Printed Flexible Electronics With High Conductivity. *Nanoscale* **2014**, *6*, 1622–1628.
- (25) Tai, Y.-L.; Yang, Z.-G. Preparation of Stable Aqueous Conductive Ink With Silver Microflakes and Its Application on Paper-Based Flexible Electronics. *Surf. Interface Anal.* **2012**, *44*, 529–534.
- (26) Audoit, J.; Laffont, L.; Lonjon, A.; Dantras, E.; Lacabanne, C. Percolative Silver Nanoplates/PVDF Nanocomposites: Bulk and Surface Electrical Conduction. *Polymer* **2015**, *78*, 104–110.
- (27) Lee, Y.-L.; Kim, S.; Jung, S.-B.; Myung, N. V.; Choa, Y.-H. Enhanced Electrical and Mechanical Properties of Silver Nanoplatelet-Based Conductive Features Direct Printed on a Flexible Substrate. *ACS Appl. Mater. Interfaces* **2013**, *5*, 5908–5913.
- (28) Russo, A.; Ahn, B. Y.; Adams, J. J.; Duoss, E. B.; Bernhard, J. T.; Lewis, J. A. Pen-on-Paper Flexible Electronics. *Adv. Mater.* **2011**, *23*, 3426–3430.
- (29) Langley, D. P.; Lagrange, M.; Giusti, G.; Jimenez, C.; Brechet, Y.; Nguyen, N. D.; Bellet, D. Metallic Nanowire Networks: Effects of Thermal Sintering on Electrical Resistance. *Nanoscale* **2014**, *6*, 13535–13543.
- (30) Hu, L.; Kim, H. S.; Lee, J.-Y.; Peumans, P.; Cui, Y. Scalable Coating and Properties of Transparent, Flexible, Silver Nanowire Electrodes. *ACS Nano* **2010**, *4*, 2955–2963.
- (31) Garnett, E. C.; Cai, W.; Cha, J. J.; Mahmood, F.; Connor, S. T.; Greyson Christoforo, M.; Cui, Y.; McGehee, M. D.; Brongersma, M. L. Self-Limited Plasmonic Welding of Silver Nanowire Junctions. *Nat. Mater.* **2012**, *11*, 241–249.
- (32) Lee, J.-Y.; Connor, S. T.; Cui, Y.; Peumans, P. Solution-Processed Metal Nanowire Mesh Transparent Electrodes. *Nano Lett.* **2008**, *8*, 689–692.
- (33) Mutiso, R. M.; Sherrott, M. C.; Rathmell, A. R.; Wiley, B. J.; Winey, K. I. Integrating Simulations and Experiments To Predict Sheet Resistance and Optical Transmittance in Nanowire Films for Transparent Conductors. *ACS Nano* **2013**, *7*, 7654–7663.
- (34) Song, T.-B.; Chen, Y.; Chung, C.-H.; Yang, Y.; Bob, B.; Duan, H.-S.; Li, G.; Tu, K.-N.; Huang, Y.; Yang, Y. Nanoscale Joule Heating and Electromigration Enhanced Ripening of Silver Nanowire Contacts. *ACS Nano* **2014**, *8*, 2804–2811.
- (35) Ye, S.; Rathmell, A. R.; Chen, Z.; Stewart, I. E.; Wiley, B. J. Metal Nanowire Networks: The Next Generation of Transparent Conductors. *Adv. Mater.* **2014**, *26*, 6670–6687.
- (36) Lagrange, M.; Langley, D. P.; Giusti, G.; Jimenez, C.; Brechet, Y.; Bellet, D. Optimization of Silver Nanowire-Based Transparent Electrodes: Effects of Density, Size and Thermal Sintering. *Nanoscale* **2015**, *7*, 17410–17423.
- (37) Borchert, J. W.; Stewart, I. E.; Ye, S.; Rathmell, A. R.; Wiley, B. J.; Winey, K. I. Effects of Length Dispersity and Film Fabrication on the Sheet Resistance of Copper Nanowire Transparent Conductors. *Nanoscale* **2015**, *7*, 14496–14504.
- (38) Bergin, S. M.; Chen, Y.-H.; Rathmell, A. R.; Charbonneau, P.; Li, Z.-Y.; Wiley, B. J. The Effect of Nanowire Length and Diameter on the Properties of Transparent, Conducting Nanowire Films. *Nanoscale* **2012**, *4*, 1996–2004.